Competition between wall slip and shear banding in wormlike micelles

M. Paul Lettinga[1, *] and Sébastien Manneville[2]

[1]*IFF, Institut Weiche Materie, Forschungszentrum Jülich,D-52425 Jülich, Germany*

[2]*Laboratoire de Physique, Université de Lyon – École Normale Supérieure de Lyon – CNRS UMR 5672 46 allée d'Italie, F-69364 Lyon cedex 07, France*

(Dated: March 16, 2009)

The interplay between shear band (SB) formation and boundary conditions is investigated in wormlike micellar systems using ultrasonic velocimetry coupled to standard rheology in Couette geometry. Transient strain-controlled experiments are performed on 6 and 10 wt. % CPyCl–NaSal wormlike micelle solutions. Time-resolved velocity profiles measured in smooth and sand-blasted geometries show (i) that boundary conditions strongly influence both the dynamics of SB formation and the SB fluctuations in the steady state and (ii) evidence for metastability close to the onset of shear banding.

PACS numbers: 83.60.-a, 83.80.Qr, 47.50.+d, 43.58.+z

During the past two decades, shear banding, i.e. the shear-induced coexistence of macroscopic bands with widely different viscosities, has been evidenced in a large range of complex fluids [1]. Sheared dispersions of surfactant wormlike micelles have attracted considerable attention due to their practical use in industry, but also because they challenged the physicists to address a non-equilibrium problem with concepts from thermodynamics [1, 2]. Indeed, rheological measurements show that the flow curve of shear-banding systems, i.e. the measured shear stress σ vs. the applied shear rate $\dot{\gamma}$, presents a plateau at a well-defined shear stress $\sigma^\star$ over a given range of shear rates [3], very similar to the plateau in pressure as a function of overall concentration of a demixed system. To underline the similarities with equilibrium phase transitions, it has been suggested that the flow curve presents a kind of "van der Waals loop," including metastable and unstable regions respectively before and after the maximum. The existence of a metastable region would imply that the system has to overcome a *stress barrier* $\Delta\sigma^{\max}$ in order for shear bands (SB) to be formed.

Experimentally, startup of steady strain in various cetylpyridinium chloride/sodium salicylate (CPyCl–NaSal) micellar solutions has revealed that the stress relaxation involves slow transients suggestive of metastability and nucleation mechanisms [4, 5]. On the theoretical side, the concept of the van der Waals loop has been used to reason SB formation [6, 7]. In two recent papers [8, 9], the kinetics of SB formation in 6 wt. % CPyCl–NaSal solutions have been nicely addressed using particle imaging velocimetry and flow birefringence in Couette geometry. After a step increase of the shear rate from the linear regime into the shear-banding regime, SB were shown to form typically within one relaxation time of the micellar solution at rest. Then the local shear rate in the high-shear (low-shear resp.) band evolves to its final value $\dot{\gamma}_2$ ($\dot{\gamma}_1$ resp.), which also corresponds to the upper (lower resp.) limit of the stress plateau, while the interface between SB migrates and stabilizes at a position δ roughly consistent with the "lever rule": $\varepsilon = \delta/e = (\dot{\gamma} - \dot{\gamma}_1)/(\dot{\gamma}_2 - \dot{\gamma}_1)$, where ε denotes the proportion of the gap occupied by the highly sheared band and e the gap width. Such observations imply that the flow is unstable over the whole stress plateau and contradict the existence of a metastable part in the flow curve. Therefore the question is whether the stress barrier, a prerequisite for metastability, actually exists and, if so, how it can be accessed.

In this Letter we use *boundary conditions* (BC) at the walls as an experimental tool to probe metastability by offering the system alternative routes to release stress. We enforce "stick" BC by using a rough sand-blasted Plexiglas Couette cell and "slip" BC by using a smooth Plexiglas cell [10]. As in Refs. [8, 9], we perform shear rate quenches on semidilute 6 wt. % CPyCl–NaSal in 0.5 M NaCl brine at 23°C, which was shown to follow the SB scenario described above [8, 11]. Experiments on a 10 wt. % sample (as in [12]), closer to the equilibrium isotropic-nematic transition that occurs at about 20 wt. %, are also discussed. The competition between SB formation and wall slip is addressed through simultaneous rheological [13] and time-resolved velocity profiles measurements. For the latter, we use ultrasonic speckle velocimetry (USV) [14, 15] since the sand-blasted cell is not transparent and optical techniques as in [8, 9] would be too difficult to implement. We show that boundary conditions strongly influence both the dynamics of SB formation and the SB fluctuations in the steady state. We propose to interpret our results as the signature of a metastable branch along which wall slip can provide a way for the system to release part of the stress barrier.

The flow curve of 6 wt. % CPyCl–NaSal shown in Fig. 1(a) for stick and slip BC reveals a stress plateau at $\sigma^\star \simeq 75$ Pa that extends from $\dot{\gamma}_1 \simeq 4.5$ to $\dot{\gamma}_2 \simeq 22$ s^{-1}, with a slight tilt due to the curvature of the Couette cell [11]. Interestingly the flow curve for slip BC does not show such a sharp bend at $\dot{\gamma}_1$ as with stick BC. Fig. 1(b)

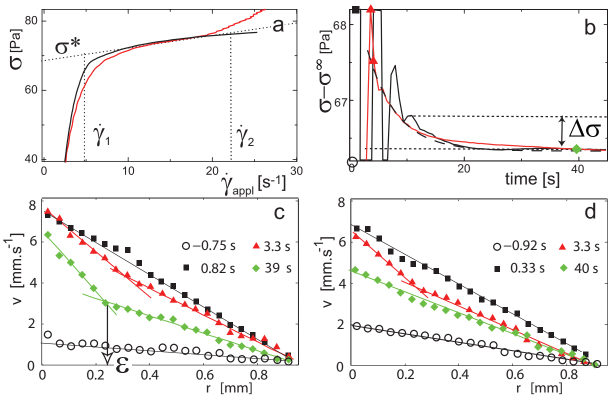

FIG. 1: (color online) (a) Steady-state flow curves of 6 wt. % CPyCl–NaSal for stick (black) and slip BC (red) for a total sweep duration of 1200 s. (b) Stress responses $\sigma(t)-\sigma^\infty$ after a shear rate quench to $\dot\gamma_{\rm appl} = 8$ s^{-1} at $t = 0$ for stick (black, $\dot\gamma_{\rm init} = 0.8$ s^{-1}) and slip BC (red, $\dot\gamma_{\rm init} = 2$ s^{-1}). The dashed line indicates an exponential decay with a characteristic time of 10 s. (c) Velocity profiles $v(r, t)$ for stick BC at various times during the quench shown in (b) (see colored dots in (b)). r denotes the radial position from the inner rotating cylinder. (d) Same as (c) for slip BC.

presents the stress responses for quenches from $\dot\gamma_{\rm init}$ located in the low shear regime to $\dot\gamma_{\rm appl} = 8$ s^{-1} located in the *beginning* of the stress plateau. Conform to earlier experiments [4, 5], the stress shows a slow decay after an initial overshoot followed by a few oscillations. As in Ref. [5], we define the amplitude of this slow relaxation as $\Delta\sigma = \sigma^M - \sigma^\infty$, where σ^M is the "mechanical" stress at the end of the oscillations and σ^∞ is the steady-state shear stress. Although the initial overshoot is far more pronounced for stick BC, the stress responses for $t \gtrsim 10$ s are very similar for both BC. Yet, depending on the BC, velocity profiles display radically different behaviors that persist in the steady state. As seen from Fig. 1(c) and (d), linear profiles are recorded just before and after the shear rate quench for both BC. For stick BC, a shear band develops within a few seconds with $\varepsilon \simeq 0.5$ and migrates towards its final position in agreement with previous observations [8]. For slip BC, however, shear banding is observed only *transiently* (see the velocity profile at $t = 3.3$ s in Fig. 1(d)) and the steady state is characterized by a *homogeneous* shear flow with a large amount of wall slip (about 40 %) at the inner cylinder.

Figure 2 provides the analysis of the time-resolved velocity measurements after the quenches of Fig. 1. Each velocity profile was analyzed to extract the true shear rate $\dot\gamma_{\rm true}$, the proportion of highly sheared material ε, and the local shear rates $\dot\gamma_\pm$ in each SB [16]. As noted above our results for stick BC are consistent with previous data where no significant wall slip was reported [8, 11]. They also unveil two important new features: (i) the presence of noticeable fluctuations in both $\dot\gamma_{\rm true}(t)$ and $\dot\gamma_+(t)$ while $\varepsilon(t)$ and $\dot\gamma_-(t)$ remain roughly constant

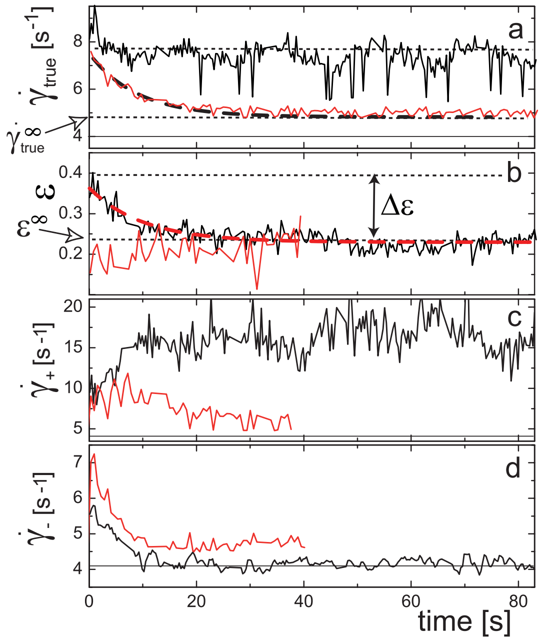

FIG. 2: (color online) Analysis of the velocity data corresponding to the shear rate quenches of Fig. 1 with stick (black) and slip BC (red). (a) True shear rate $\dot\gamma_{\rm true}(t)$. (b) Proportion of the high SB $\varepsilon(t)$. (c) Shear rate in the high SB $\dot\gamma_+(t)$ and (d) in the low SB $\dot\gamma_-(t)$. The dashed lines indicate exponential decays with the same time constant of 10 s.

for $t \gtrsim 30$ s and (ii) the fact that the position of the SB settles with the same dynamics as the shear stress. For slip BC, Fig. 2(a) shows that (i) the imposed shear rate $\dot\gamma_{\rm appl}$ cannot be sustained although $\dot\gamma_{\rm true} \simeq \dot\gamma_{\rm appl}$ at early times and (ii) wall slip sets in with the same time constant as the stress relaxation since $\dot\gamma_{\rm true}(t)$ and $\sigma(t)$ follow the same decay. Fig. 2(b) and (c) reveal that shear banding is observed during the build up of wall slip. Here a high SB is formed with $\varepsilon \simeq 0.2$ and $\dot\gamma_+ \simeq 10$ s^{-1}, a value close to the initial shear rate for stick BC. However, for slip BC, $\dot\gamma_+$ rapidly drops and approaches $\dot\gamma_-$, which leads to the loss of banding structure (hence the lack of $\varepsilon(t)$ and $\dot\gamma_\pm$ data for $t \gtrsim 40$ s) and to linear profiles with $\dot\gamma_{\rm true} \simeq 5$ s^{-1} in the steady state. For a shear rate quench to $\dot\gamma_{\rm appl} = 8$ s^{-1}, we conclude that two stress relaxation processes are competing: wall slip vs SB formation. Both processes have the same time constants since the decay of $\dot\gamma_{\rm true}(t)$ for slip BC is the same as the settling of the SB through $\varepsilon(t)$ for stick BC. As a consequence the stress relaxations for stick and slip BC are also similar (see the dashed line in Fig. 1(b)).

Quenches were repeated as described above for final shear rates $\dot\gamma_{\rm appl}$ covering almost the whole stress plateau [17]. Figure 3 presents the steady state values of the true shear rate $\dot\gamma^\infty_{\rm true}$ and of the proportion of the high SB ε^∞, as well as the amplitude of the relaxation of $\varepsilon(t)$ (noted $\Delta\varepsilon$ and defined in Fig. 2(b)) and that of the stress relaxation $\Delta\sigma$. As shown by the solid line $\dot\gamma_{\rm true} = \dot\gamma_{\rm appl}$

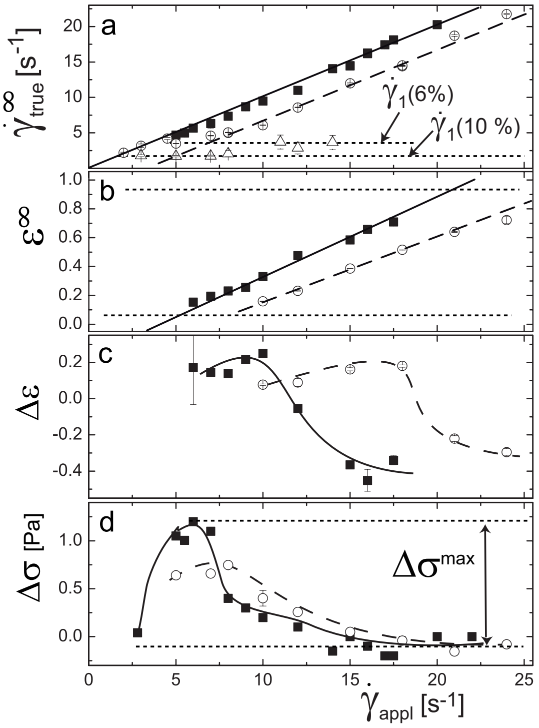

FIG. 3: Steady state values of (a) the true shear rate $\dot{\gamma}^{\infty}_{\rm true}$ and (b) the proportion of the high SB ε^{∞}, and amplitudes of the relaxations of (c) the proportion of the high SB $\Delta\varepsilon$ and (d) the shear stress $\Delta\sigma$ as a function of the imposed shear rate $\dot{\gamma}_{\rm appl}$ for stick (solid symbols) and slip BC (open symbols). All data are for 6 wt. % CPyCl–NaSal except for the triangles in (a) which are for 10 wt. % CPyCl–NaSal with slip BC. In (a) the solid line is $\dot{\gamma}_{\rm true} = \dot{\gamma}_{\rm appl}$, while the dashed line is $\dot{\gamma}_{\rm true} = \dot{\gamma}_{\rm appl} - 3.4$ s^{-1} and the dotted lines indicate $\dot{\gamma}_1$ for 6 and 10 wt. % CPyCl–NaSal. The dotted lines in (b) show the resolution limit for SB detection [16]. The lines in (c) and (d) are to guide the eye.

in Fig. 3(a), stick BC are valid for the sand-blasted cell. Moreover the linear behavior of ε^{∞} vs. $\dot{\gamma}_{\rm appl}$ is consistent with the lever rule (see solid line in Fig. 3(b)) and leads to $\dot{\gamma}_1 = 3.4 \pm 0.2$ s^{-1} and $\dot{\gamma}_2 = 22.4 \pm 0.5$ s^{-1} in satisfactory agreement with both the flow curve and the steady states values of the local shear rates $\dot{\gamma}_- = 4.3 \pm 0.3$ s^{-1} and $\dot{\gamma}_+ = 22 \pm 1$ s^{-1}. Note also that $\dot{\gamma}_-$ and $\dot{\gamma}_+$ increase somewhat with increasing $\dot{\gamma}_{\rm appl}$ (data not shown). These observations not only confirm previous results in the absence of wall slip [8, 9, 11] but also allow us to evidence the migration of the high SB towards the stator (i.e. $\Delta\varepsilon < 0$) for deep quenches, since we were able to access the upper part of the flow curve.

For slip BC, $\dot{\gamma}_{\rm true} = \dot{\gamma}_{\rm appl}$ only holds when $\dot{\gamma}_{\rm appl} < \dot{\gamma}_1$. Wall slip is always observed for $\dot{\gamma}_{\rm appl} > \dot{\gamma}_1$ and $\dot{\gamma}^{\infty}_{\rm true}$ is shifted by a constant $\Delta\dot{\gamma} \simeq 3.4$ s^{-1} with respect to stick BC. If SB occurs in the presence of wall slip, then one expects ε^{∞} to be shifted by the same amount. Figure 3(b) shows that SB indeed sets in for $\dot{\gamma}_{\rm appl} \simeq \dot{\gamma}_1 + \Delta\dot{\gamma} \simeq 7$ s^{-1}. However the slope of ε^{∞} vs $\dot{\gamma}_{\rm appl}$ is noticeably smaller than for stick BC leading to a shift that increases with $\dot{\gamma}_{\rm appl}$ (see dashed line in Fig. 3(b)). The same observation holds for Fig. 3(c) where the shift between the $\Delta\varepsilon$ curves is seen to increase up to about 15 s^{-1} for the highest achievable $\dot{\gamma}_{\rm appl}$. This suggests a more subtle influence of wall slip on SB than a mere shift due to the difference between $\dot{\gamma}_{\rm appl}$ and $\dot{\gamma}_{\rm true}$. In particular, this points to a larger value of $\dot{\gamma}_2$ for slip BC, which is indeed hinted by the velocity profiles (not shown) but remains questionable due to surface instability for very deep quenches.

Finally, if one assumes that the slip layer at the rotor is characteristic of the shear-induced structure sheared at $\dot{\gamma}_+ \simeq \dot{\gamma}_2$, i.e. that its viscosity does not depend on $\dot{\gamma}_{\rm appl}$ throughout the stress plateau, then a constant $\Delta\dot{\gamma}$ corresponds to some *constant stress* released by wall slip. Within the stress barrier picture described in the introduction, the most natural interpretation is that this stress release is used to lower the stress barrier. Figure 3(d) shows that $\Delta\sigma^{\rm max}$ is about twice smaller for slip BC than for stick BC. At larger $\dot{\gamma}_{\rm appl}$, the excess stress follows roughly the same decay for both BC. We conclude that about half the stress barrier is released through wall slip with our "smooth" BC.

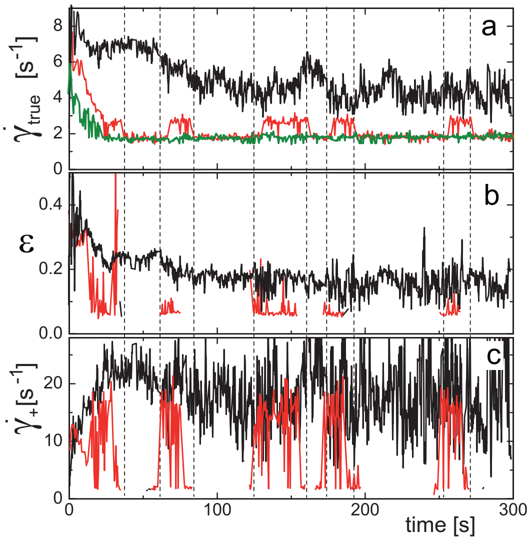

FIG. 4: (color online) Responses to shear rate quenches from $\dot{\gamma}_{\rm init} = 0.8$ s^{-1} to $\dot{\gamma}_{\rm appl} = 8$ s^{-1} for stick (black) and slip BC (red) in 10 wt. % CPyCl–NaSal. (a) True shear rate $\dot{\gamma}_{\rm true}(t)$. The green line is the response to a quench to $\dot{\gamma}_{\rm appl} = 5$ s^{-1} for slip BC. (b) Proportion of the high SB $\varepsilon(t)$. (c) Shear rate in the high SB $\dot{\gamma}_+(t)$. The vertical dashed lines indicate the times where SB nucleate and melt (see text).

The large fluctuations of $\dot{\gamma}_{\rm true}$ and $\dot{\gamma}_+(t)$ in Fig. 2 suggest that small slip events might still occur even with stick BC, hinting that stick BC are only valid up to some degree. In order to toughen the competition between SB and wall slip, a 10 wt. % CPyCl–NaSal sample, for which $\sigma^{\star} \simeq 158$ Pa, $\dot{\gamma}_1 \simeq 1.7$ s^{-1}, and $\dot{\gamma}_2 \simeq 20$ s^{-1}, was submitted to shear rate quenches as analyzed in Fig. 4. Even in the sand-blasted cell where stick BC are supposed to be valid, the true shear rate never coincides with $\dot{\gamma}_{\rm appl}$. For slip BC and $\dot{\gamma}_{\rm appl} = 5$ s^{-1}, we observe that the sample slips to the shear rate $\dot{\gamma}_1$ at the start of the stress plateau where there is no excess stress (see the green line in Fig. 4(a)). Moreover a quench to a somewhat higher shear rate of $\dot{\gamma}_{\rm appl} = 8$ s^{-1} reveals hints of "nucleation and melt" events: over short time windows indicated by vertical dashed lines in Fig. 4, $\dot{\gamma}_{\rm true}$ jumps from $\dot{\gamma}_1$ to significantly higher values. Velocity profiles also show that, when $\dot{\gamma}_{\rm true} > \dot{\gamma}_1$, a small but detectable high SB forms with $\varepsilon \gtrsim 0.1$ and $\dot{\gamma}_+ \simeq 15$–20 s^{-1}. Such "nucleation and melt" behavior, where the new state is formed over short periods of time and is unstable over longer times, is typical of metastability as known from classical thermodynamics. Since $\dot{\gamma}_{\rm true} \approx \dot{\gamma}_1$ up to $\dot{\gamma}_{\rm appl} \simeq 12$ s^{-1} (see open triangles Fig. 3(a), where large error bars are due to the nucleation events), we conclude that, for the 10 wt. % CPyCl–NaSal sample, the metastable region extends over a large part of the stress plateau and that slip is the most direct way to release stress, so that stable SB can only be formed when stick BC are enforced in an even more rigorous way than in the present experiments.

In conclusion, combined velocimetry and rheology confirm the analogy between the SB instability in wormlike micelles and classical thermodynamics. Tuning the boundary conditions allowed us to explore metastable and unstable regimes and to evidence for the first time the analogue of "nucleation and melt" events. Wall slip was shown to provide a way to release at least part of the stress barrier and BC appear as a crucial control parameter which could account for some of the fluctuations reported in earlier measurements on similar systems [12, 18]. The influence of BC on SB formation was addressed theoretically in two recent papers [19, 20], with emphasis on hysteresis and shear history dependence. Here we found no clear difference between quench up or quench down (data not shown), hinting that anchoring to the walls is similar in both SB. Still our results call for more theoretical effort, particularly on the influence of BC on the dynamics and fluctuations of SB.

Finally the question remains open of what the microscopic analogue of a nucleation site may be. In earlier papers , it was suggested that a small highly sheared band at the rotating wall could play the role of a heterogenous nucleus. Due to our limited resolution on ε, we cannot provide any support for this assumption. Alternatively spatially localized "stick" sites could also promote nucleation. To confirm this idea, one should explore the flow in the close vicinity of the cell walls by using microscopic techniques, e.g. in microfluidic devices.

The present experiments were funded by the EU SoftComp Network of Excellence and performed at Centre de Recherche Paul Pascal, Pessac, France. The authors thank P. Ballesta, E. Laurichesse, and S. Lerouge for technical help and J. K. G. Dhont and P. D. Olmsted for fruitful discussions.

* Electronic address: `p.lettinga@fz-juelich.de`

[1] See the recent reviews by S. M. Fielding, Soft Matter **3**, 1262 (2007); J. K. G. Dhont and W. Briels, Rheol. Acta **47**, 257 (2008); P. D. Olmsted, Rheol. Acta **47**, 283 (2008), and references therein.
[2] J.-F. Berret *et al.*, J. Phys. II France **4**, 1261 (1994).
[3] H. Rehage and H. Hoffmann, Mol. Phys. **74**, 933 (1991).
[4] C. Grand *et al.*, J. Phys. II France **7**, 1071 (1997).
[5] J.-F. Berret, Langmuir **13**, 2227 (1997).
[6] J. K. G. Dhont, Phys. Rev. E **60**, 4534 (1999).
[7] P. D. Olmsted *et al.*, J. Rheol. **44**, 257 (1999).
[8] Y. T. Hu and A. Lips, J. Rheol. **49**, 1001 (2005).
[9] E. Miller and J. P. Rothstein, J. Non-Newtonian Fluid Mech. **143**, 22 (2007).
[10] Our "smooth" ("rough" resp.) walls have a roughness (average standard deviation of height profiles measured from atomic force microscopy) of 15 nm (0.6 μm resp.).
[11] J.-B. Salmon *et al.*, Phys. Rev. Lett. **90**, 228303 (2003).
[12] M. R. López-González *et al.*, Phys. Rev. Lett. **93**, 268302 (2004).
[13] Rheological data are collected with a stress controlled rheometer (TA Instruments AR 1000) in Couette cells with inner radius 24 mm, outer radius 25 mm, and height 30 mm. A computer-controlled feedback loop is used to apply quenches between constant shear rates and the corresponding stress response $\sigma(t)$ is recorded.
[14] S. Manneville *et al.*, Eur. Phys. J. Appl. Phys. **28**, 361 (2004).
[15] USV yields velocity profiles across the gap of the Couette cells at about 15 mm from the cell bottom with a spatial resolution of 40 μm and a temporal resolution of 0.1 s. USV requires that the acoustically transparent micellar samples be seeded with 0.7 wt. % hollow glass spheres (Sphericel, Potters) of mean diameter 6 μm that scatter ultrasound. We checked that this does not significantly affect the rheology of our samples.
[16] Velocity profiles are linearly extrapolated to estimate the fluid velocities close to the walls $v(0,t)$ and $v(e,t)$, yielding $\dot{\gamma}_{\rm true}(t) = (v(0,t) - v(e,t))/e$. The intersection and the slopes of linear fits of $v(x,t)$ over the two SB respectively yield the position $\delta(t) = e\,\varepsilon(t)$ of the interface between SB and the local shear rates $\dot{\gamma}_+(t)$ and $\dot{\gamma}_-(t)$. Due to the USV spatial resolution, this fitting procedure cannot ascertain the presence of SB smaller than 80 μm, hence the lack of data points with $\varepsilon \lesssim 0.1$ in Fig. 3(b).
[17] Such a large shear rate range, as compared to Refs. [8, 9], was achieved by using a special lid that reduces the air-sample interface in order to hinder instability of the free surface which results in air inclusions for deep quenches.
[18] L. Bécu *et al.*, Phys. Rev. Lett. **93**, 018301 (2004).
[19] J. M. Adams *et al.*, J. Non-Newtonian Fluids Mech. **115**, 101 (2008).
[20] L. F. Rossi *et al.*, J. Non-Newtonian Fluids Mech. **136**, 79 (2006).